RSC Advances

Accepted Manuscript

This article can be cited before page numbers have been issued, to do this please use: K. Tang, J. Zhu, Y. Ye, Y. Tang and L. Chen, *RSC Adv.*, 2016, DOI: 10.1039/C6RA23474G.

ROYAL SOCIETY OF CHEMISTRY

rsc.li/rsc-advances

View Article Online
DOI: 10.1039/C6RA23474G

RSC Advances

ARTICLE

Efficient Hydrogenation of Dimethyl Oxalate to Ethylene Glycol *via* Nickel Stabilized Copper Catalysts

Received 00th January 20xx,
Accepted 00th January 20xx

DOI: 10.1039/x0xx00000x

www.rsc.org/

Junhua Zhu,[a,b] Yingchun Ye,[b] Yi Tang,[*,a] Liangfeng Chen[b] and Kangjian Tang,[*,b]

$CuNi/SiO_2$ nanocatalysts with Ni-stabilized Cu nanoparticles around 10 nm were synthesized. After H_2 reduction, the catalysts with grain size around 25 nm showed very high performance on catalytic hydrogenation of dimethyl oxalate to ethylene glycol at a mild reaction condition. The composition and structure of these nanocatalysts were characterized. It is shown that Ni played a key role in stabilizing Cu against deactivation. To meet the requirement of industrial application, the optimal $CuNi/SiO_2$ nanocatalyst was tested under continuous reaction for over 2000 hours. The conversion and product selectivity maintained at 99% and above 95%, respectively.

Introduction

With the depletion of crude oil resources and increasing environmental concerns, developing alternative economical and energy-efficient processes is very imperative.[1] Producing chemicals from syngas is one of the most promising routes. Ethylene glycol (EG),[2] as one of the largest global producing and consuming chemicals,[3] catalyzed from syngas has been studied intensely within recent years.[4-8] Industrial process of syngas to EG (STE) currently involves three steps: 1) obtaining high-pure carbon monoxide (CO), 2) coupling of CO by using of nitrite esters to dimethyl oxalates (DMO)[9] and 3) selective hydrogenation of DMO to EG.[10-11] The selective hydrogenation of DMO to EG is the key reaction in the STE route which has drawn much attention of industry and academia. As shown in Scheme. 1, DMO with three kinds of active groups (C=O, C-O and CH_3-O) could lead to some different reaction routes. The methyl glycolate ($C_3H_6O_3$) is the preliminary state, which could lead to an equilibrium reaction with the product of b_2 and lead to aimed product, EG. Based on EG, an over hydrogenation could lead to EtOH (b_1) easily and an acidic/basic catalysis could lead to unexpected polymerization, such as b_3 or b_4 *etc*[12]. To meet the industrial demands, the catalysts for hydrogenation of DMO to EG must possess some following properties: 1) high conversion rate and high selectivity to EG, 2) high stability for service life, 3) running no more than 270°C in case of unexpected over-polymerization. [13]

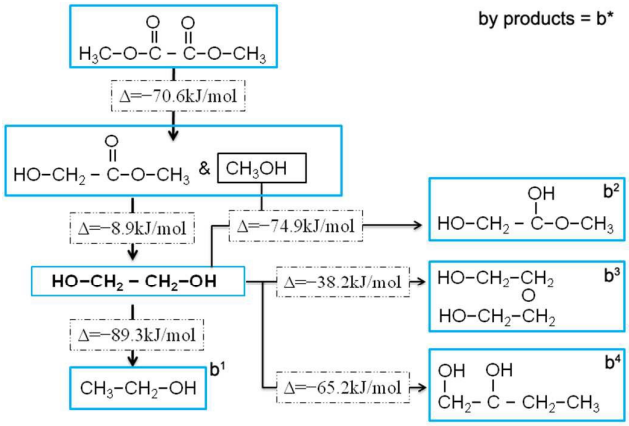

Scheme 1. The proposed reaction pathways of DMO hydrogenation.

Cu-based catalyst has been regarded as a good candidate and well investigated, which could trigger the reaction at mild conditions with high conversion and less coke. Some works performed on supports,[14-18] some works on assisted agents[19-23] and some works on the acid-base properties[12, 24] were reported. However, as Cu-based catalyst is very sensitive to reaction temperature and impurities in raw material, the selectivity and stability of copper catalysts are always the key problems for industry. Generally, the activity of Cu-based catalyst is extremely low below 200 °C and easily deactivates over 230 °C because of the coke and aggregation of Cu nanoparticles.[25] To meet the industrial requirements, it is important to improve the activity by stabilizing Cu or decrease the reaction temperature, such as Ni-based bimetal system.[26-28] So far, the efficient Cu-based catalyst is still hard to be developed. In our previous work, we reported the facile method to fabricate copper-nickel surface sites and disperse highly on the SiO_2 with grain size around 10 nm in diameter. The Cu^{+}-$Ni^{\delta}O_x$ surface sites greatly improved the catalytic performance on hydrogenation of LA or ethyl-levulinate (EL) to γ-valerolactone under mild-condition.[29] Here, we report the development of STE results based on such Cu-Ni-Si

[a] Department of Chemistry, Fudan University, Shanghai 200433, (P.R. China) Fax: +86-21-65641740; Tel: +86-21-55664125 yitang@fudan.edu.cn
[b] Shanghai Research Institute of Petrochemical Technology, SINOPEC, Shanghai, 201208 (P. R. China). Fax: +86-21-68462283; Tel: +86-21-68462197-1202; E-mail: tangkj.sshy@sinopec.com
[c] Footnotes relating to the title and/or authors should appear here.
Electronic Supplementary Information (ESI) available: [details of any supplementary information available should be included here]. See DOI: 10.1039/x0xx00000x

View Article Online
DOI: 10.1039/C6RA23474G

system. With this kind of catalysts, the catalysis could maintain high activity (over 99% conversion and 95% selectivity) for over 2000 hours without decay, which well meets the requirements of industry.

Results and discussion

Figure 1 showed the H_2-TPR profiles of the series of $CuNi/SiO_2$ samples. For the $CuNi(0)/SiO_2$ sample, the temperature of the main reduction peak was 219.1 °C. With the introduction of Ni, the main reduction peak gradually changed to lower temperature, which was 211.5 °C when the Ni amount was 8%. This phenomenon illustrated that there existed some kind of interaction between Cu-Ni-Si, which had also been observed by Zhao et al. [30], this interaction made the Ni-containing catalysts more easily to be reduced than $CuNi(0)/SiO_2$.

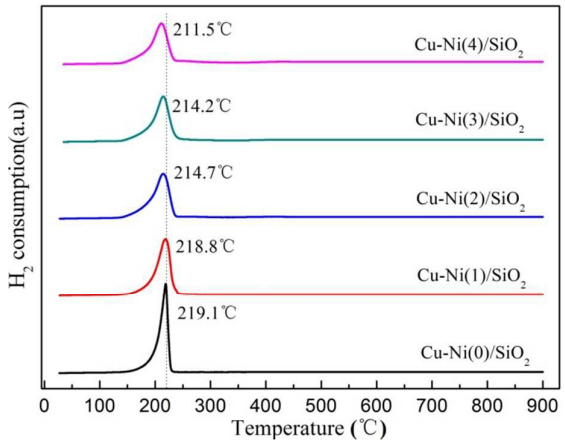

Figure 1. H_2-TPR profiles of as-prepared catalysts.

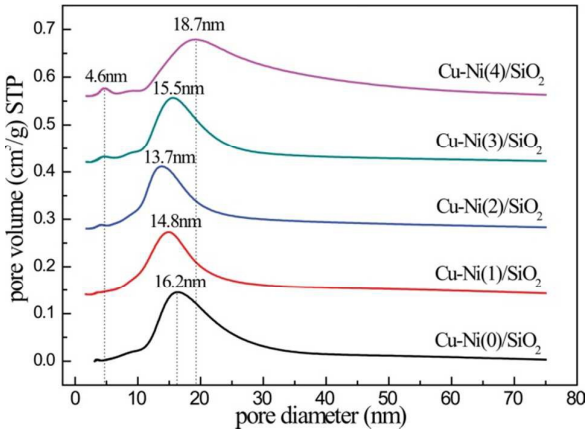

Figure 2. Pore size distribution of as-prepared catalysts.

The pore size distribution curves (shown in Figure. 2) exhibited a wide bimodal distribution around 15.0 nm, and 4.6 nm when the Ni was introduced. It can be prospected that the large volume around 15.0 nm could solve the problem of coke well. Interestingly, the nickel-modified Cu/SiO_2 has new a pore diameter as 4.6 nm, indicating that the textural structure of the catalyst was determined not only by the copper species but also by the nickel species. Meanwhile, the change of wide distribution decreased from 16.2 nm to 13.7 nm and then increased to 18.7 nm implies there is a threshold for the introduced amount of Ni.

Figure 3a and 3b showed the compared X-ray diffraction (XRD) patterns of as-prepared and reduced samples of $CuNi(0\sim4)/SiO_2$. Without Ni species, the XRD showed characteristic peaks of CuO and chrysocolla ($Cu_{2-x}Si_2O_5(OH)_x$ structures on as-prepared sample. The Cu and Cu_2O structures would be recorded after reduction by H_2. With the introduction of Ni, the chrysocolla structure collapsed by steps and all CuO structures remained when the amount of Ni over 4%. That's to say, the introduction of Ni could restrict observably the crystallization of chrysocolla. Since the peaks at around 37° are affiliated to both Cu_2O and NiO and the peaks at around 43° are affiliated to Cu or NiO, we have to identify the structures of Ni and Cu species based on the peaks at 50.4° and 62.8°, after H_2 reductions. From the reduced XRD results, the peaks affiliating to metal Cu were very obvious but the peaks corresponding to copper oxides and nickel oxides were not so clear. The calculation by Scherrer Formula gave the particle size as 12.7, 16.9, 25.3, 25.7 and 25.9 nanometers from $CuNi(0)/SiO_2$ to $CuNi(4)/SiO_2$. One important observation was that the Cu particle size increased with the increasing of induced amount of Ni.

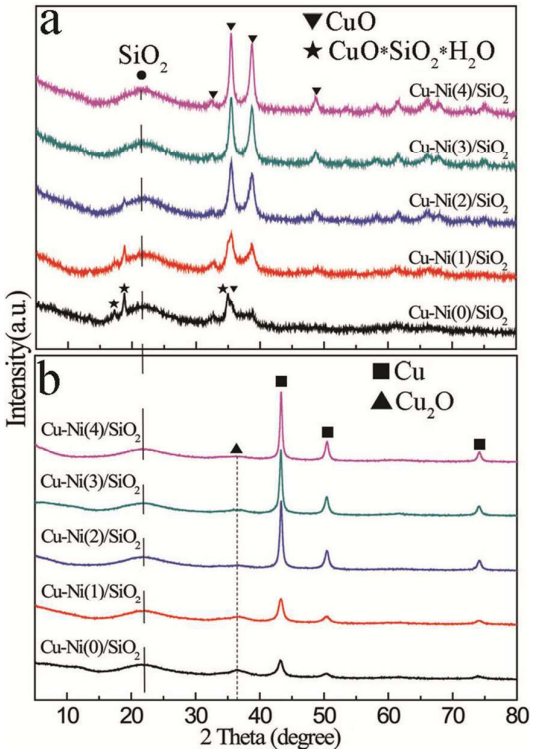

Figure 3. XRD curves of (a) as-prepared and (b) H_2 reduced catalysts.

View Article Online
DOI: 10.1039/C6RA23474G

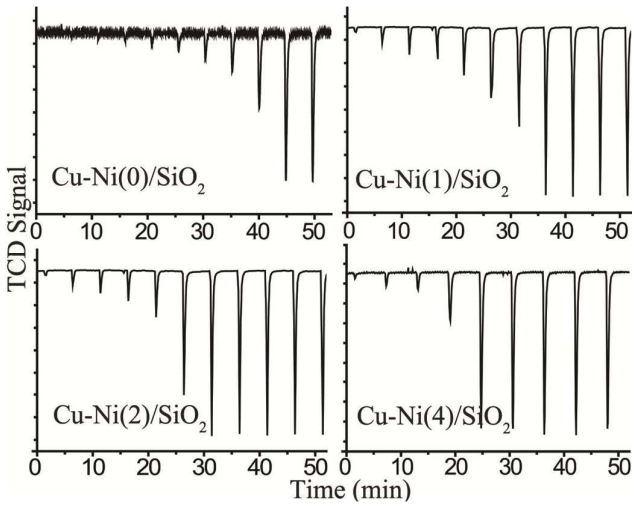

Figure 4. Pulse consumption of H_2 on series of $CuNi/SiO_2$ catalysts.

Figure 4 displayed the H_2 consumption by pulse method. By comparing the series of $CuNi/SiO_2$ catalysts, the consumption number on $CuNi(0)/SiO_2$, $CuNi(1)/SiO_2$, $CuNi(2)/SiO_2$ and $CuNi(4)/SiO_2$ were 7.7, 5.5, 4.5 and 3.4, respectively. Corresponding Cu dispersion could be calculated to 7.5%, 5.6%, 4.7%, and 3.4%, respectively. The particle size was calculated to 14.3nm, 17.8nm, 23.0nm and 31.0nm, which were in agreement with XRD results.

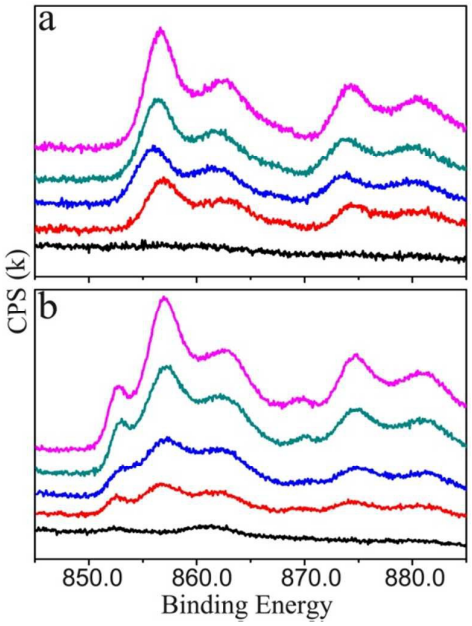

Figure 5. Ni2p3/2 XPS diagram of (a) before and (b) after reduction. Series of $CuNi/SiO_2$ catalysts with different Ni content were showed as different color. black line: Ni(0), red line: Ni(1), blue line: Ni(2), green line: Ni(3), pink line: Ni(4).

Figure 5 compared the valent state of Nickel in series of catalysts before and after reduction. As can be seen from Fig. 5a, virtually all nickel species in the four catalysts exists as Ni^{2+}. After reduction by H_2, most nickel remained as Ni^{2+} (Fig. 5b), however, One small new peak occurred at about 853 eV, implying that a few Ni^{2+} species have been partly reduced to Ni^{1+}, which may be adjacent to Cu species, acting as stabilizers to Cu nanoparticles. Meanwhile, no peak at 852.3 eV was found in XPS, which means that no Ni^0 exists in reduced $CuNi/SiO_2$ catalysts. Figure 6 showed the catalytic performance of the $CuNi/SiO_2$ catalysts with different ratio of Cu to Ni in gas-phase hydrogenation of DMO. Steady-state product compositions were obtained after 120 h on stream. It is known that the hydrogenation of DMO proceeds *via* methyl glycolate (MG) to EG, while EG can dehydrate further to ethanol (Scheme 1). The reaction between EG and ethanol on basic sites yields 1,2-BDO.[31] As shown in Table 1, the conversion of DMO increased with increased introduced Ni amount from 97.33% on the $CuNi(0)/SiO_2$ to 99.99% on catalyst $CuNi(2)/SiO_2$, and then decreased slightly to 95.63% on the $CuNi(4)/SiO_2$ catalyst. Almost all the converted DMO had been turned into MG and EG. The selectivities to ethanol remained <1% and no 1,2-BDO was detected. Figure 6 compared activities on different particle size as well. In traditional, the smaller size of the Cu nanoparticles is, the better performance should be obtained. But, our catalysis results showed that the Cu particle with the size about 25 nm had much better catalytic performance than that with 14 nm. As known, in the year of 2007, an innovative discovery regarding shape-dependent catalysis was made, which was heralded as the new face of catalysis.[32] Research showed that "different atom arrays naturally display crystallographically distinct facets, whose surface atoms have distinct catalytic activities".[33] Our results implies that the introduction of Ni into Cu-based catalysts made the Cu has more specific surfaces to catalyze the DMO to final products.

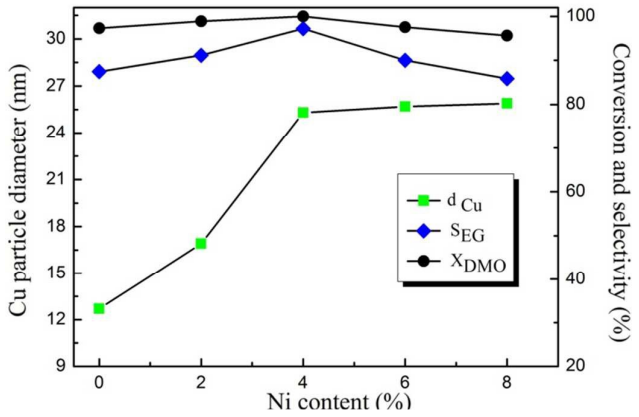

Figure 6. Effect of the Ni amount and Cu particles size on the catalytic performance of the $CuNi/SiO_2$ catalysts. Reaction conditions: 3.0 MPa, 215°C, and H_2/DMO ratio 100 (mol/mol), $LHSV_{DMO}$ = 0.55h^{-1}

Table 1. The DMO hydrogenation performance of catalysts with different Ni content

Catalyst	X_{DMO}, %	S_{EG}, %	S_{MG}, %	S_{EtOH}, %
$Cu-Ni(0)/SiO_2$	97.33	87.47	9.24	0.45
$Cu-Ni(1)/SiO_2$	98.90	91.16	6.24	0.84
$Cu-Ni(2)/SiO_2$	99.99	97.22	1.45	0.75
$Cu-Ni(3)/SiO_2$	97.54	90.01	3.79	0.63
$Cu-Ni(4)/SiO_2$	95.63	85.88	6.71	0.38

View Article Online
DOI: 10.1039/C6RA23474G

Note： X-conversion， S-selectivity. Reaction conditions: 215°C, 3.0Mpa, H_2/DMO = 100(mol/mol), $LHSV_{DMO}$ = 0.55h^{-1}. The data were acquired after reaction for 120 hours.

Upon the investigations from XRD, XPS, chemisorptions and reactions, it could be speculated (as shown in schematic scheme 2.) that without the introduction of nickel, the Cu species is unstable during the reaction and easy to aggregate to be bigger grains due to the weak interaction between copper and silica. When small amount of nickel, were introduced, the Ni-O species could insert between Cu and Si species, result in the stabilization of Cu species. With further increasing of the nickel content, an optimized dispersion of Cu could be obtained based on the threshold of dispersing Ni-O species on silica. However, excess introduction of nickel lead to the aggregation of nickel oxide, on which the tiny copper sites had the chance of over growth.

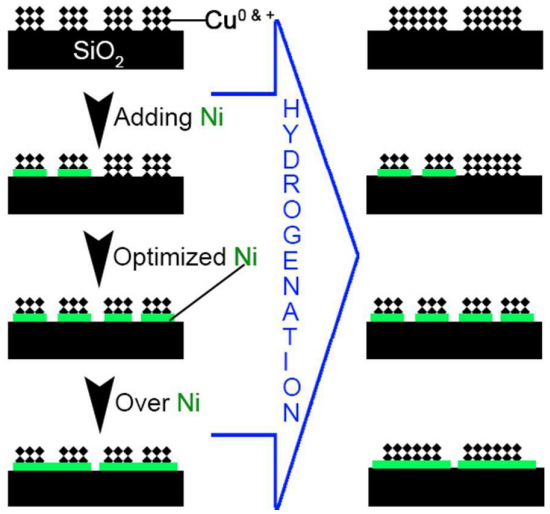

Scheme 2. Schematic model for the variation of Cu species with increased nickel content.

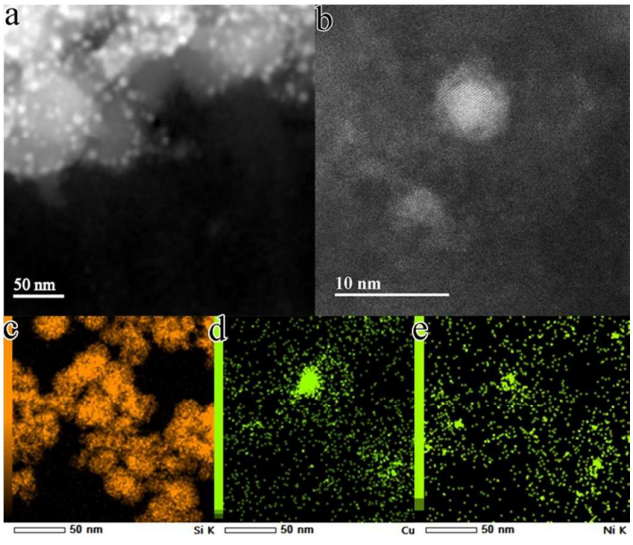

Figure 7. (a) and (b) HRSTEM images and (c)-(e) STEM-EDS elemental mapping on a 50nm domain of CuNi(2)/SiO_2 catalyst.

Since the CuNi(2)/SiO_2 exhibited the highest hydrogenation efficiency, it was chosen to perform further observation and practical catalytic hydrogenation of DMO to EG. High resolution aberration-corrected scanning transmission electron microscopy (HRSTEM) images (Figure 7a and b) revealed the activities on substrates are very fine nanoparticles with about 10 nm diameter. Figure 7c~e show the EDX mapping analysis on 50 nm domain, which reveal that the copper and nickel were mixed well on the SiO_2 surface and the appearance of Cu was always coupled with the presence of Ni. The HRSTEM observation was in agreement to our speculation on scheme 2. Figure 8 displayed the detailed catalytic results on the optimized CuNi(2)/SiO_2 catalyst. During the 2000 hours test, we investigated its conversion, temperature-dependent selectivity, stability and distribution of byproducts. The CuNi(2)/SiO_2 catalyst could hold its over 99% conversion and 95% selectivity at the temperature from 215 °C to 230 °C without any decay.

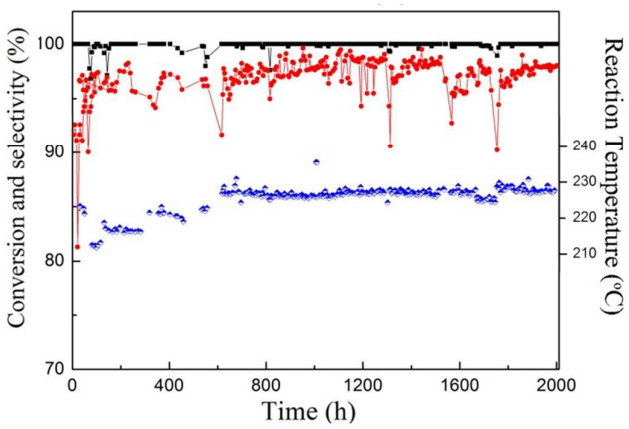

Figure 8. Catalytic performance and stability test of optimized CuNi(2)/SiO_2 catalyst at from 215°C to 230°C, 3.0 MPa, H_2/DMO ratio 100 (mol/mol), $LHSV_{DMO}$ = 0.55h^{-1}. Conversion, selectivity and temperature were shown by black red and blue lines, respectively.

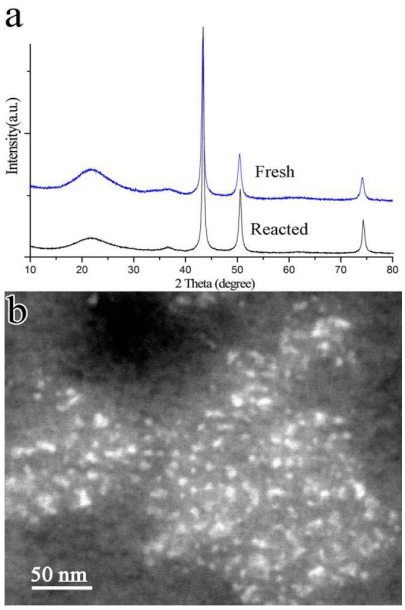

Figure 9. (a) XRD curve and (b) STEM image of reacted CuNi(2)/SiO_2 catalyst.

View Article Online
DOI: 10.1039/C6RA23474G

The nature of the catalyst after 2000 hours' test was then recorded by XRD and STEM. Figure 9a showed the compared XRD curves on fresh H_2-reduced and reacted $CuNi(2)/SiO_2$ catalyst. Two samples have full same featured peaks, meaning the reacted one keeping original structure unchanged. Shaper peak implies the particle size of reacted one is a little larger than fresh one. With Scherrer Formula, the particle size of reacted one could be calculated to 26.5 nm. Figure 9b showed the STEM image. The average particles' size was around 25 nm and separated obviously. Both the results revealed the catalyst's activites be able to hold its particle size and dispersibility, and corresponding its super stability.

Conclusions

In conclusion, Cu-based model catalysts by adding nickel to improve performance have been explored for the reaction of DMO to EG. The appropriate amount of nickel could be vital for the optimized catalysis. The Ni-O species can effectively stabilize Cu and is ideal for using in industry as its over 99% conversion, 95% selectivity, and over 2000 hours' stability. The strategy for the synthesis of stable mixed oxides provides a simple method in catalyst preparation and selectivity control. Results from the current study demonstrate the high potential to synthesize mixed metal oxides catalysts for practical applications.

Experimental

The Cu-based catalysts were prepared by a co-precipitation method in which 0.20M aqueous solution of $Cu(NO_3)_2.3H_2O$, $Ni(NO_3)_2.3H_2O$ and proper amount of silica sol were taken and precipitated using 0.2M aqueous sodium carbonate at ambient temperature. The precipitate was aged further for 8 h at 60 ºC. Then the mixture was separated by filtration and washed with deionized water to remove the traces of sodium. The solid thus obtained was dried in static oven at 110 ºC for 24 h and calcined at 400 ºC for 4 h. The weight percentage of copper in the Cu/SiO_2 catalyst was hold as 35%. The samples name as $CuNi(0)/SiO_2$ without introducing Ni and CuNi(1~4)/SiO2 with introducing amount of Ni as 2%, 4%, 6% and 8%.

X-ray powder diffraction **(XRD)** patterns on series of catalysts were recorded in the range of 5~80° on Bruker D8 diffractometer using Cu Kα radiation with a scanning step 0.002°, voltage 40kV, and current 100mA. High resolution Transmission Electron Microscopy **(TEM)** was recorded on a FEI TECNAI-20 instrument with accelerating voltage of 200 kV. TEM specimen was prepared by dispersing the powder in alcohol by ultrasonic treatment and dropping onto a holey carbon film supported on a copper grid, and then dried in air. Scanning transmission electron microscopy **(STEM)** was performed on a double-corrected Titan Cubed 60-300 and a cold field emission gun was operated at 200 kV. STEM images were recorded using a high-angle annular dark-field (HAADF) detector. Temperature Programmed Reduction (**TPR**) was performed on a Micromeritics AutoChem 2950; N_2 adsorption (BET and pore size analysis) was performed on a Micromeritics ASAP2000M. The dispersion and metallic copper surface areas of the catalysts were determined by N_2O **CHEMISORPTION** at 333 K according to the literature.[34] 100 mg of Cu-based catalysts calcined at 623 K was reduced by 5% H_2-95% Ar (25mL/min) at 623 K for 2 h and cooled to 333 K. Then pure N_2O was introduced to oxidize Cu atoms completely on the surface. $2Cu\ (s) + N_2O \rightarrow Cu_2O\ (s) + N_2$. The quantity of irreversibly chemisorbed O_2 atoms was measured by a hydrogen pulse chromatographic technique on a Micromeritics Autochem II 2920 equipped with a TCD. Hydrogen pulse-dosing was repeated until there has no change. The consumed amount of hydrogen was the value obtained by subtracting the small area of the first few pulses from the area of the other pulses. Copper loading of all reduced catalysts was analyzed by X-ray fluorescence **(XRF)** on a Bruker S4 Pioneer. Copper dispersion was calculated by dividing the amount of chemisorption sites into total supported copper atoms. X-ray photoelectron spectroscopy **(XPS)** studies were performed on a Kratos AXIS Ultra DLD spectrometer equipped with a high temperature gas reaction cell. All the spectra were well collected with monochromatic Al K_α The C 1s peak at 284.8 eV was set as reference for binding energy calibration. All the spectrum processing and peak fitting were performed with CasaXPS.

All the reactions were carried out in a continuous flow, fixed-bed reactor and 5g catalysts were packed in the reactor. Prior to the reaction, the catalyst was reduced at 260 ºC in H_2 flow. DMO and H_2 were fed into the reactor using an injection pump, and the LHSV flow rate of DMO was 0.55 h^{-1}. The reaction temperature was adjusted between 210ºC and 230ºC. The reaction pressure was maintained at 3.0 MPa. The molar ratio of H_2 to DMO was set as 100 (mol/mol). The hydrogenation products were analyzed using gas chromatography (Agilent 7890) equipped with a flame ionization detector and a capillary column (DB-200). The main products and byproducts were identified by GC-MS method on Agilent 5975C inert XL EI/CI MSD.

Acknowledgements

The authors thank the partially financial support from the SINOPEC, National Natural Science Foundation of China (NSFC 21373272 and 2013CB93410).

References

1. G. W. Huber, S. Iborra and A. Corma, Chem. Rev., 2006, **106**, 4044–4098.
2. M. W. Forkner, J. H. Robson, W. M. Snelling, A. E. Martin, F. H. Murphy and T. E. Parsons, Glycols–Ethylene Glycols, 2004.
3. World Petrochemical (WP) report on Ethylene Glycol http://chemical.ihs.com/WP/Public/Reports/eg/.
4. A. Y. Yin, X. Y. Guo, W. L. Dai and K. N. Fan, Chem. Commun., 2010, **46**, 4348–4350.
5. Z. He, H. Q. Lin, P. He and Y. Z. Yuan, J. Catal., 2011, **277**, 54–63.
6. A. Yin, C. Wen, X. Guo, W. L. Dai and K. Fan, J. Catal., 2011, **280**, 77–88.
7. A. Yin, X. Guo, W. Dai and K. Fan, J. Phys. Chem. C, 2009, **113**, 11003–11013.
8. G. Xu, Y. Li, Z. Li and H. Wang, Ind. Eng. Chem. Res., 1995, **34**, 2371–2378.
9. Z. Xu, J. Sun, C. Lin, X. Jiang, Q. Chen, S. Peng, M. Wang, G. Guo, Acs Catal. 2013, **3**, 118-123..
10. L. Chen, P. Guo, M. Qiao, S. Yan, H. Li, W. Shen, H. Xu and K. N. Fan, J. Catal., 2008, **257**, 172–180.
11. Y. Huang, H. Arig, X. Zheng, X. Duan, S. Takakusagi, K. Asakur, Y. Yuan, J. Catal. 2013, **307**, 74–83.
12. Y. Song, J. Zhang, J. Lv, Y. Zhao, and Xinbin Ma，Ind. Eng. Chem. Res. 2015, **54**, 9699–9707.
13. S. G. Hovenkamp, J. P. Munting, J. Polym. Sci A, 1970, 8, 679-682
14. J. Ding, J. Zhang, C. Zhang, K. Liu, H. Xiao, F. Kong, J. Chen, Appl. Catal. A: General 2015, **508**, 68–79.
15. C. Wen, A. Yin, Y. Cui, X.Yang, W. Dai, K. Fan ; Appl. Catal. A: General 2013, **458**, 82– 89.
16. A. Yin, X. Guo, W. Dai, H. Li, K. Fan，Appl. Catal. A: General 2008, **349**, 91–99.
17. Y. Zhu, Y. Zhu, G. Ding, S. Zhu, H. Zheng, Y. Li, Appl. Catal. A: General 2013, **468**, 296– 304.

View Article Online
DOI: 10.1039/C6RA23474G

18. H. Lin, X. Duan, J. Zheng, X. Zheng, P. He, Y. Yuan and Y. Yang , RSC Adv., 2013, **3**, 11782–11789.
19. S. Zhao, H. Yue, Y. Zhao, B. Wang, Y. Geng, J. Lv, S. Wang, J. Gong, X. Ma , J. Catal. 2013, 297, 142–150.
20. Z. He, H. Lin, P. He, Y. Yuan , J. Catal. 2011, 277, 54–63.
21. X. Zheng, H. Lin, J. Zheng, X. Duan, and Y. Yuan, ACS Catal. 2013, **3**, 2738−2749.
22. H. Miyazaki, T. Uda, K. Hirai, Y. Nakamura, H. Ikezawa, T. Tsuchie, 1986, US4585890
23. A. Yin, J. Qu, X. Guo, W. Dai, K. Fan , Appl. Catal. A: General 2011, 400, 39–47.
24. Y. Zhu, X. Kong, X. Li, G. Ding, Y. Zhu, and Y. Li, ACS Catal. 2014, **4**, 3612−3620.
25. B. Putrakumar, N. Nagaraju, V.P. Kumar, K.V.R. Chary, Catal. Today, 2015, **250**, 209–217.
26. J. Zhang, M. Ibrahim, V. Collière, H. Asakura, T. Tanaka, K. Teramura, K. Philippot, N.Yan. J. Mol. Catal. A: Chemical 2016, **422**, 188–197.
27. J. Zhang, J. Teo, X. Chen, H. Asakura, T. Tanaka, K. Teramura, N. Yan. Acs Catal., 2014, **4**, 1574-1583.
28. S. De, J. Zhang, R. Luque, N. Yan. Energy Environ. Sci., 2016, **9**, 3314-3347.
29. J. Zhu, Y. Tang and K. Tang, RSC Adv., 2016, **6**, 87294-87298.
30. Y. Zhao, S. Zhao, Y. Geng, Y. Shen, H. Yue, J. Lv, S. Wang, X. Ma, Catal. Today, 2016, 276, 28-35
31. C. Carlini, M.D. Girolamo, A. Macinai, J. Mol. Catal. A 2003, **200**, 137-145.
32. D. L. Feldheim, Science 2007, **316**, 699.
33. P.D. Yang, Nature 2012, **41**, 482-483.
34. C.J.G. Van Der Grift, A.F.H. Wielers, B.P.J. Jogh, J. Van Beunum, M. De Boer, M. Versluijs-Helder, J.W. Geus, J. Catal. 1991, **131**, 178-188.